physica status solidi b

phys. stat. sol. (b) **243**, No. 8, 1922–1928 (2006) / **DOI** 10.1002/pssb.200541167

Magnetic and magnetotransport properties in $(La_xSm_{1-x})_{2/3}Sr_{1/3}MnO_3$ (x = 1/3, 1/2 and 2/3) manganites

Saket Asthana[1], **A. K. Nigam**[2], and **D. Bahadur**[*, 1]

[1] Department of Metallurgical Engineering and Materials Science, Indian Institute of Technology, Mumbai 400076, India

[2] Tata Institute of Fundamental Research, Colaba, Mumbai 400005, India

Received 19 July 2005, revised 4 January 2006, accepted 2 March 2006
Published online 5 May 2006

PACS 61.10.Nz, 71.38.+k, 75.47.Lx

The magnetic and transport properties of $(La_xSm_{1-x})_{2/3}Sr_{1/3}MnO_3$ (x = 1/3, 1/2 and 2/3) manganites, prepared by the citrate-gel route, have been investigated. These compounds are found to crystallize in the orthorhombic structure. The hopping between Mn^{3+} and Mn^{4+} sites is controlled by the Mn–O–Mn bond angle. The magnetoresistance in 8.5 kOe fields varies from 15 to 25 percent over the temperature range 300 K to 80 K. The conduction mechanism can be understood by using the correlated small polaron model. The metal–insulator as well as magnetic transition temperatures are close to each other, which indicates the dominance of long-range ferromagnetic ordering in the present system. At low temperatures, a weak ferromagnetic to antiferromagnetic transition is indicated, which could be due to competing superexchange and double exchange interactions. The charge localization at lower temperatures could be the possible explanation for increasing magnetoresistance. The maximum magnetic moment at 5 K, for all the samples is ~3.6μ_B/Mn, which is close to the 3.7μ_B/Mn, as obtained by considering the Mn spins only.

1 Introduction

The manganites have attracted the attention of researchers from the technological as well as theoretical point of view. The mixed valance perovskites are well known for exhibiting negative colossal magnetoresistance (CMR) as well as very rich phase diagrams. The richness in crystal structure and physical properties is due to the subtle competition between charge, orbital, spin and phonon degrees of freedom [1, 2]. The other interesting property in manganites is the presence of coexisting clusters of competing phases. These phases are typically ferromagnetic and different kinds of antiferromagnetic phases. The generation of these competing phases is a strong function of the overlap integral caused by mixing cations of different size at A site.

The properties of manganites can be tuned by introducing cations at the A or B sites or varying the oxygen content [3–5]. Mixing cations of different ionic radii at the A site is the most straightforward experimental method for a systematic tuning of the properties of these materials. The variation in the average ionic radius at A site, $\langle r_A \rangle$, leads to competing phases at particular temperature. The present series $(La_xSm_{1-x})_{2/3}Sr_{1/3}MnO_3$ (x = 1/3, 1/2 and 2/3) has been chosen to study the influence of varying rare earth ion concentration at A site on the physical properties of the system.

[*] Corresponding author: e-mail: dhirenb@iitb.ac.in

Original Paper

2 Experimental details

Polycrystalline $(La_xSm_{1-x})_{2/3}Sr_{1/3}MnO_3$ (x = 1/3, 1/2 and 2/3) samples were synthesized by the chemical citrate-gel route using high-purity La_2O_3, Sm_2O_3, $SrCO_3$ and manganese acetate. The as-prepared powders were calcined at 1000 °C in air for 2 h. The powders were pelletized and sintered at 1200 °C in air. X-ray diffraction patterns of the samples were recorded using Cu K_α radiation (PW3040/60 Philips, PANalytical). Resistivity measurements were carried out from 300 to 20 K using the standard four-probe dc method. Magnetic measurements were made using a vibrating sample magnetometer (Oxford, Maglab VSM) at a 100 Oe field in the temperature range 300–5 K.

3 Results and discussion

All the samples in series $(La_xSm_{1-x})_{2/3}Sr_{1/3}MnO_3$ (x = 1/3, 1/2 and 2/3) crystallize in the orthorhombic crystal system. The peaks shift towards the lower-angle side, which leads to an increase in the cell volume of the unit cell as observed with increasing tolerance factor. The tolerance factor is defined as $[\langle r_A \rangle + r_O]/[\sqrt{2}\ (r_B + r_O)]$, where $\langle r_A \rangle$ is the average A-site ionic radii. The structure is refined by using the Rietveld refinement method [6]. The refinement was carried out in the space group Pnma (No. 62) with the following atomic positions: La/Sm/Sr: 4c(x, y, 1/4), Mn: 4b(0, 0, 1/2), O(1): 4c(x, 1/4, z) and O(2): 8d(x, y, z). A typical refined pattern of the sample with x = 2/3 is shown in Fig. 1. The goodness of fitting parameter, S (= R_{wp}/R_{exp} where R_{wp} is the weighted profile factor and R_{exp} is the expected weighted profile factor) is in the range of 1.2–1.52. The refined lattice parameters and tolerance factor are summarized in Table 1.

The electrical resistivity behavior with temperature for the series $(La_xSm_{1-x})_{2/3}Sr_{1/3}MnO_3$ (x = 1/3, 1/2 and 2/3) is shown in Fig. 2. The metal–insulator transition is observed in all the compositions. The T_{MI} shifts to lower temperatures with decreasing La^{3+} ion (IR = 1.36 Å) content due to the disorder created by substituting smaller size Sm^{3+} (1.24 Å) ion. The average ionic radius at A site increases from 1.33 Å (x = 1/3) to 1.36 Å (x = 2/3) which suppresses the MnO_6 distortion within the lattice. The mean radius has been calculated using the coordination number twelve [7]. The tolerance factor increases with increasing La^{3+} content as a result of which MnO_6 octahedra gets more symmetric and the resistivity decreases due to the Mn–O–Mn bond angle, which approaches 180° [8]. The hopping between Mn^{3+} and Mn^{4+} sites is controlled by the Mn–O–Mn bond angle. The transfer integral, defined as $t = t_0 \cos(\theta/2)$, where t_0 comes from the parallel arrangement of the spins and θ is the angle between the core spins [2].

The transfer integral increases, as the system attains the Mn–O–Mn angle approaching 180° and facilitates the double exchange (DE), which leads to the decrease in resistivity. The slight upturn in the $\rho(T)$ curves at lower temperatures due to charge localization behavior is observed as shown in inset of Fig. 2. The two competing effects at lower temperatures are charge localizations, which favors the canted antiferromagnetic spin arrangement and the hopping integral, which is controlled by DE interaction.

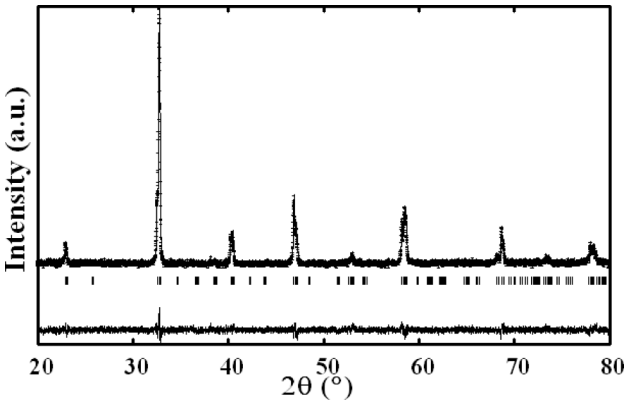

Fig. 1 Observed and fitted X-ray diffraction pattern of the sample $(La_{2/3}Sm_{1/3})_{2/3}Sr_{1/3}MnO_3$.

Table 1 Refined lattice parameters using the Rietveld method, tolerance factors 'τ', T_{MI} and T_C for the series, $(La_xSm_{1-x})_{2/3}Sr_{1/3}MnO_3$ (x = 1/3, 1/2 and 2/3). The theoretical fitted parameters are also given.

x	a (Å)	b (Å)	c (Å)	V (Å)^3	τ	T_{MI} (K)	T_C (K)	n (10^{21}/cc)	ε_p (K)	U_0 (K)	θ (K)
1/3	5.4722 (3)	7.7063 (8)	5.4599 (2)	230.25 (1)	0.960	196	205	1.5	500	700	80
1/2	5.4812 (4)	7.7073 (5)	5.4572 (1)	230.54 (2)	0.966	238	270	1.3	380	460	84
2/3	5.4962 (5)	7.7053 (7)	5.4582 (8)	231.15 (4)	0.971	258	315	1.4	196	380	30

The conduction mechanism over the entire temperature range from 300–20 K could be understood by the correlated small polaron model [9]. The expression for dc hopping resistivity is derived from the Holstein Hamiltonian by considering the electron–phonon and spin–spin relaxation times and activation energy U, which is associated with the formation of the magnetic polaron. The expression for dc resistivity is given by

$$\rho_{\text{hop}}^{c} = \left[\frac{AT}{n} \left\{ 1 + c\left(1 - m^2(t)\right) \sigma_a^2 \right\} \cosh^2\left(\frac{\varepsilon_p}{2(T+\theta)} \right) \exp\left(\frac{U}{T} \right) \right], \tag{1}$$

$$A = \frac{1.13 k_B}{\omega_{ph} a^2 e^2}. \tag{2}$$

Here, n is the density of charge carriers, ω_{ph} (5×10^{12} Hz) is the frequency of the longitudinal optical phonon and a is the hopping distance. The σ_a is the short-range order parameter that depends on the atomic ordering temperature (T_{ca}) which is fixed at 310 K, θ is the low-temperature vibrational energy, ε_p is the small polaron stabilization energy and U is the activation energy, $U = U_0(1 - m^k)\ \sigma_a^2$. The c and k are constants depending on the strength of the spin–spin scattering in polaron transport. Here U_0 is the constant, k varies from 2.3 (for x = 1/3) to 3.5 (for x = 2/3) and m is obtained by solving $m = \tan h(m/t)$, where $t = T/T_{MI}$, applicable for a system that has only two stable spin states. The conduction mechanism is well explained in A site [10] as well as B site [11] substituted manganites. This model is valid over the entire temperature range from 300 to 20 K, irrespective of metallic or insulating phase. The number of variables used earlier in this model has now been reduced to only U_0, ε_p and θ and k by keeping the other parameters fixed. The theoretical fitted curves are also shown in Fig. 2. All the parameters obtained from the above fitting including T_{MI} are given in Table 1. The systematic decrease in U_0 as well as ε_p is observed with increasing La^{3+} content, which indicates that the energy required to overcome the hopping barrier also reduces. The slight upturn also observed in the fitted plots reflects the presence of charge

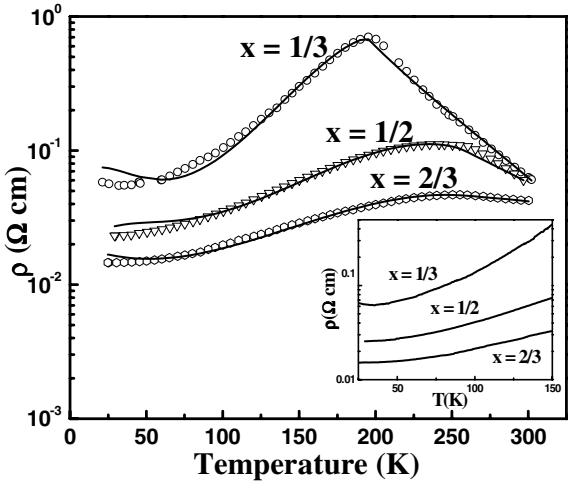

Fig. 2 Variation of resistivity with temperature for the series $(La_xSm_{1-x})_{2/3}Sr_{1/3}MnO_3$ (x = 1/3, 1/2 and 2/3). Fitted plots are indicated by the solid line. The inset shows the charge localization behavior at lower temperatures.

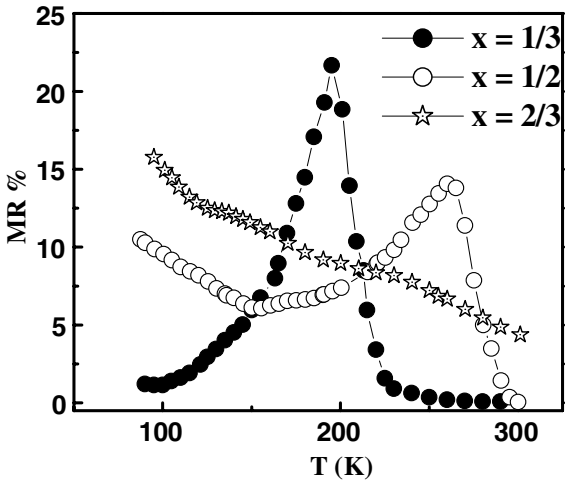

Fig. 3 Variation of MR with temperature in a field of 8.5 kOe for $(La_xSm_{1-x})_{2/3}Sr_{1/3}MnO_3$ (x = 1/3, 1/2 and 2/3) samples.

localization at lower temperatures. The density of charge carriers is almost invariable with La^{3+} content because of a fixed Sr^{2+} concentration.

The magnetoresistance behavior of the above series in a field of 8.5 kOe is shown in Fig. 3. In the presence of an external field, the resistivity decreases significantly. The decrement in resistivity suggests that the external magnetic field facilitates the hopping of e_g electrons between neighbouring Mn ions, which agrees with the DE model [12, 13]. The magnetoresistance (MR) is defined as

$$\%\mathrm{MR} = 100 \times [\rho(H, T) - \rho(0, T)]/[\rho(0, T)] \,, \tag{3}$$

where $\rho(H, T)$ and $\rho(0, T)$ are the resistivities at a temperature T, in applied magnetic field H and in zero applied magnetic field, respectively. The highest MR (~25%) is observed in the sample with x = 1/3 at T_{MI}. Except for sample with x = 2/3, rest two samples show maximum MR at T_{MI}. The manganese ions start aligning ferromagnetically below T_{MI}; therefore, within a single magnetic domain, the e_g electron transfer between Mn^{3+} and Mn^{4+} ions is easy. The pairs of Mn^{3+} and Mn^{4+} spins, which may not be parallel in the vicinity of domain wall boundaries, will act as a hindrance for electron transport. The magnetic domains tend to align along the field direction in the presence of sufficiently strong magnetic field. The broad maxima at T_{MI} for the sample with x = 2/3 may be the reason for the different MR behavior. The suppression of charge localization in the presence of magnetic field will facilitate the e_g electron hopping and will in turn continuously decrease the resistivity at lower temperatures. This may be the possible

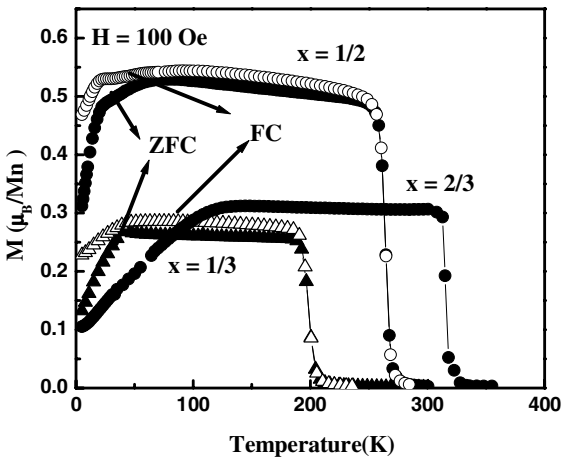

Fig. 4 Magnetization as a function of temperature for the series $(La_xSm_{1-x})_{2/3}Sr_{1/3}MnO_3$ (x = 1/3, 1/2 and 2/3) in a 100 Oe field.

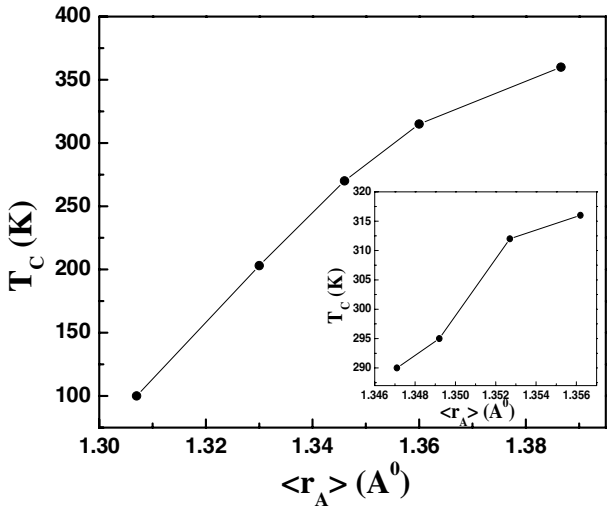

Fig. 5 Variation of T_C with the average ionic radius at A site for series $(La_xSm_{1-x})_{2/3}Sr_{1/3}MnO_3$ (x = 1/3, 1/2 and 2/3). The data for end members x = 0 and 1 have been taken from Refs. [19] and [20], respectively. The inset shows the same variation for the series $La_{2/3-x}Pr_xSr_{1/3}MnO_3$ [18].

reason for the increasing MR at lower temperatures especially in samples with x = 1/2 and 2/3. The overall MR behavior could be attributed to an intergrain tunneling mechanism [14].

The variation of magnetization (M) with temperature (T) for the series $(La_xSm_{1-x})_{2/3}Sr_{1/3}MnO_3$ (x = 1/3, 1/2 and 2/3) in a field of 100 Oe is shown in Fig. 4. Except for the sample with x = 2/3, other samples exhibit paramagnetic (PM) to ferromagnetic (FM) transition below room temperature. T_C is determined by the point of inflexion in the M–T plots and is included in Table 1. T_{MI} and T_C in all the three cases are nearly comparable. This indicates that the long-range ferromagnetic ordering is well established in these systems [15]. The difference between T_C and T_{MI} increases with La^{3+} content, which indicates that the charge localization effect at lower temperatures is more prominent in the sample with x = 2/3. This is also observed in the MR behavior. A weak ferromagnetic to antiferromagnetic (AFM) transition is also observed in all the cases due to localization of the charge carriers. The bifurcation in zero field-cooled (ZFC) and field-cooled (FC) magnetization is attributed to the competing AFM and FM interactions [16]. The insignificant thermal irreversibility behavior in ZFC and FC M(T) plots is observed in the x = 1/2 and 1/3 samples, supporting the dominance of FM interaction (DE) over AFM interaction (SE) as shown in the Fig. 4. The T_C variation with $\langle r_A \rangle$ shown in Fig. 5, follows the established phase diagram [17]. The inset shows the same variation of T_C with $\langle r_A \rangle$ for the series $La_{2/3-x}Pr_xSr_{1/3}MnO_3$ as reported elsewhere [18].

The overall magnetic behavior may be explained by de Gennes [11] model according to which the Curie temperature for a ferromagnetic spin arrangement in $La_{1-x}Ca_xMnO_3$ is given by

$$k_B T_C = \frac{2}{3}[z_a |J^a| - z_b |J^b| - z_c |J^c|] S^2 + \frac{2xz\xi_p}{5}, \quad (4)$$

where z_i (i = a, b, c) are the numbers of nearest neighbours along the a-, b-, c-directions, z is the total number of nearest neighbours and J^i is the effective exchange integral in the i direction and ξ_p is the gain in energy due to hopping. The spin arrangement for ξ_p = 250 K is that of a collinear ferromagnet for $x > 0.26$ [7]. The first term in Eq. (4) comes from the antiferromagnetic and the second term is due to the ferromagnetic interaction, namely double exchange. The value of x is 0.33, which is fixed in our case. Taking J^a = 1.61 meV, $J^b = J^c$ = 0.62 meV, ξ_p = 250 K, z = 6, the T_C is 215 K for $(La_{1/3}Sm_{2/3})_{0.67}Sr_{0.33}MnO_3$, which is close to the experimental value of 205 K. The drop in the magnetization could be explained by the antiferromagnetic interaction below a particular temperature.

Figure 6 shows an isothermal magnetization plots at 5 K for the series. $(La_xSm_{1-x})_{2/3}Sr_{1/3}MnO_3$ (x = 1/3, 1/2 and 2/3). The M_S values (estimated on the basis of Mn spins only) are 3.48μ_B/Mn atom (x = 1/3), 3.58μ_B/Mn atom (x = 1/2) and 3.59μ_B/Mn atom (x = 2/3). The M_S values are very close to the theoretical

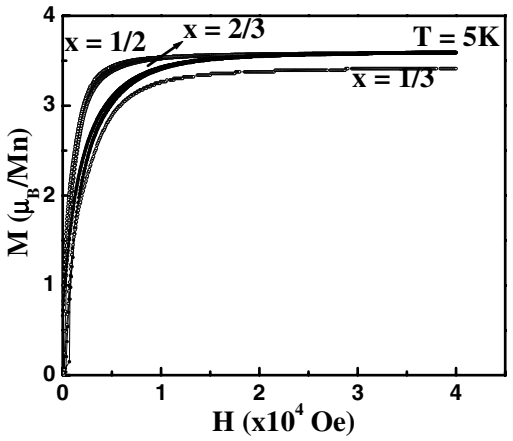

Fig. 6 Isothermal magnetization behavior with field at 5 K for series $(La_xSm_{1-x})_{2/3}Sr_{1/3}MnO_3$ (x = 1/3, 1/2 and 2/3).

value of 3.7μ_B/Mn for pure $La_{0.7}Ca_{0.3}MnO_3$. The hysteretic behavior is almost insignificant in these compositions, which indicate the soft ferromagnetic feature. The saturating MH behavior also confirms the dominance of long-range ferromagnetic ordering in these systems.

4 Conclusions

The magnetic and transport properties of the series $(La_xSm_{1-x})_{2/3}Sr_{1/3}MnO_3$ (x = 1/3, 1/2 and 2/3) have been studied. All systems are crystallized in the orthorhombic structure with space group Pnma. The MnO_6 distortion increases with decreasing average A-site ionic radii as reflected in the transport behavior. The charge localization is observed at lower temperatures both in transport and magnetic data. The correlated small polaron model could be a possible model to explain the conduction mechanism in both insulating as well as metallic regimes. The reduction in the variable parameters in this model has been helpful in improving the understanding of transport mechanism. The T_{MI} as well as T_C increases with La content. The difference between these two leads to charge localization, which could be a possible reason for the low-temperature MR. The M_S of all the compositions are almost close to the theoretical value of 3.7μ_B/Mn. The nearly similar T_{MI} and T_C in all the cases as well as saturating MH behavior indicate the dominance of ferromagnetic ordering over the antiferromagnetic ordering.

Acknowledgements Two of the authors (S.A. and D.B.), are thankful to the Department of Science and Technology (DST) India for support of the project.

References

[1] E. L. Nagaev, Phys. Rep. **346**, 387 (2001).
[2] C. N. R. Rao and B. Raveau, Colossal Magnetoresistance, Charge Ordering and Related Properties of Manganese Oxides (World Scientific, Singapore, 1998).
[3] J. P. Attfield, Cryst. Eng. **5**, 427 (2002).
[4] Y. Tokura, H. Kuwahara, Y. Moritomo, Y. Tomioka, and A. Asamitsu, Phys. Rev. Lett. **76**, 3184 (1996).
[5] A. Maignan, Ch. Simon, V. Caignaert, and B. Raveau, Z. Phys. B **99**, 305 (1996).
[6] J. Rodríguez-Carvajal, Laboratoire Léon Brillouin (CEA-CNRS) CEA/Saclay, 91191 Gif sur Yvette Cedex, France, version 2001.
[7] R. D. Shannon, Acta Crystallogr. A **32**, 751 (1976).
[8] S. Asthana, D. Bahadur, A. K. Nigam, and S. K. Malik, J. Appl. Phys. **97**, 10H711 (2005).
[9] C. M. Srivastava, J. Phys.: Condens. Matter **11**, 4539 (1999).
[10] C. M. Srivastava, S. Banerjee, T. K. GunduRao, A. K. Nigam, and D. Bahadur, J. Phys.: Condens. Matter **15**, 2375 (2003).

[11] C. M. Srivastava, R. K. Dwivedi, S. Asthana, A. K. Nigam, and D. Bahadur, J. Magn. Magn. Mater. **284**, 239 (2004).
[12] C. Zener, Phys. Rev. **82**, 403 (1951).
[13] P. G. de Gennes, Phys. Rev. **118**, 141 (1960).
[14] D. Das, A. Saha, S. E. Russek, R. Raj, and D. Bahadur, J. Appl. Phys. **93**, 8301 (2003).
[15] A. Maignan, C. Martin, G. Van Tendeloo, M. Hervieu, and B. Raveau, Phys. Rev. B **60**, 15214 (1999).
[16] S. Asthana, D. Bahadur, A. K. Nigam, and S. K. Malik, J. Phys.: Condens. Matter **16**, 5297 (2004).
[17] H. Y. Hwang, S. W. Cheong, P. G. Radaelli, M. Marezio, and B. Batlogg, Phys. Rev. Lett. **75**, 914 (1995).
[18] D. Zhu, A. Maignan, M. Hervieu, S. Hebert, and B. Raveau, Solid State Commun. **127**, 551 (2003).
[19] V. Caignart, A. Maignan, and B. Raveau, Solid State Commun. **95**, 357 (1995).
[20] R. Mahesh, R. Mahendiran, A. K. Raychaudhuri, and C. N. R. Rao, J. Solid State Chem. **120**, 204 (1995).

